

RESEARCH ARTICLE

10.1002/2016JD025443

Key Points:

- We present a metric for comparing model simulations with in situ atmospheric water vapor isotope observations
- Model artifacts for temperature and humidity cannot simply explain isotope biases on top of the Greenland Ice Sheet
- All models show inability to correctly simulate the spatial structure of marine boundary layer isotopic composition

Supporting Information:

- Supporting Information S1
- Data Set 1

Correspondence to:

H. C. Steen-Larsen,
hanschr@gfy.ku.dk

Citation:

Steen-Larsen, H. C., C. Risi, M. Werner, K. Yoshimura, and V. Masson-Delmotte (2016), Evaluating the skills of isotope-enabled general circulation models against in situ atmospheric water vapor isotope observations, *J. Geophys. Res. Atmos.*, 122, doi:10.1002/2016JD025443.

Received 30 MAY 2016

Accepted 19 DEC 2016

Accepted article online 22 DEC 2016

Evaluating the skills of isotope-enabled general circulation models against in situ atmospheric water vapor isotope observations

H. C. Steen-Larsen^{1,2} , C. Risi³ , M. Werner⁴ , K. Yoshimura⁵ , and V. Masson-Delmotte² 

¹Center for Ice and Climate, University of Copenhagen, Copenhagen, Denmark, ²Laboratoire des Sciences du Climat et de l'Environnement, UMR CEA-CNRS-UVSQ/IPSL 8212, Gif-sur-Yvette, France, ³Laboratoire de Météorologie Dynamique, Paris, France, ⁴Alfred Wegener Institute, Helmholtz Centre for Polar and Marine Research, Bremerhaven, Germany, ⁵Atmosphere and Ocean Research Institute, University of Tokyo, Kashiwa, Japan

Abstract The skills of isotope-enabled general circulation models are evaluated against atmospheric water vapor isotopes. We have combined in situ observations of surface water vapor isotopes spanning multiple field seasons (2010, 2011, and 2012) from the top of the Greenland Ice Sheet (NEEM site: 77.45°N, 51.05°W, 2484 m above sea level) with observations from the marine boundary layer of the North Atlantic and Arctic Ocean (Bermuda Islands 32.26°N, 64.88°W, year: 2012; south coast of Iceland 63.83°N, 21.47°W, year: 2012; South Greenland 61.21°N, 47.17°W, year: 2012; Svalbard 78.92°N, 11.92°E, year: 2014). This allows us to benchmark the ability to simulate the daily water vapor isotope variations from five different simulations using isotope-enabled general circulation models. Our model-data comparison documents clear isotope biases both on top of the Greenland Ice Sheet (1–11‰ for $\delta^{18}\text{O}$ and 4–19‰ for d-excess depending on model and season) and in the marine boundary layer (maximum differences for the following: Bermuda $\delta^{18}\text{O} \sim 1\%$, d-excess $\sim 3\%$; South coast of Iceland $\delta^{18}\text{O} \sim 2\%$, d-excess $\sim 5\%$; South Greenland $\delta^{18}\text{O} \sim 4\%$, d-excess $\sim 7\%$; Svalbard $\delta^{18}\text{O} \sim 2\%$, d-excess $\sim 7\%$). We find that the simulated isotope biases are not just explained by simulated biases in temperature and humidity. Instead, we argue that these isotope biases are related to a poor simulation of the spatial structure of the marine boundary layer water vapor isotopic composition. Furthermore, we specifically show that the marine boundary layer water vapor isotopes of the Baffin Bay region show strong influence on the water vapor isotopes at the NEEM deep ice core-drilling site in northwest Greenland. Our evaluation of the simulations using isotope-enabled general circulation models also documents wide intermodel spatial variability in the Arctic. This stresses the importance of a coordinated water vapor isotope-monitoring network in order to discriminate amongst these model behaviors.

1. Introduction

Water stable isotopes (H_2^{16}O , HDO, H_2^{17}O , and H_2^{18}O) have been measured in precipitation and water vapor since the 1950s [Epstein and Mayeda, 1953; Dansgaard, 1953] as important tools to characterize and understand the atmospheric hydrological cycle [e.g., Yoshimura, 2015; Galewsky et al., 2016]. Due to the isotopic fractionation occurring during phase transitions, the water stable isotopic composition is an integrated product of the physical processes associated with phase change in the atmospheric hydrological cycle. The fractionation coefficients and molecular diffusivities for the individual water stable isotopes have been determined through controlled laboratory experiments for ice-vapor exchange [Majoube, 1970; Merlivat and Nief, 1967; Ellehoj et al., 2013] and liquid-vapor exchange [Majoube, 1971; Majoube, 1970; Merlivat and Nief, 1967; Barkan and Luz, 2007]. Theoretical considerations have led to parameterizations of the isotopic exchange for precipitation [Stewart, 1975], snow crystal formation [Jouzel and Merlivat, 1984; Bolot et al., 2013], ocean evaporation [Craig and Gordon, 1965; Merlivat and Jouzel, 1979], and evapotranspiration from terrestrial vegetation [Wang and Yakir, 2000]. These parameterizations have been implemented in a growing number of general circulation models equipped with water stable isotopes (e.g., LMDZiso [Risi et al., 2010], ECHAM5-wiso [Werner et al., 2011], isoGSM [Yoshimura et al., 2008], CAM [Lee et al., 2007], and HadCM3 [Tindall et al., 2009]) and in Regional Circulation Models (RCMs) (e.g., REMOiso [Sturm et al., 2005], COSMOiso [Pfahl et al., 2012], and isoRSM [Yoshimura et al., 2010]).

In the rest of this manuscript, we will be using the delta notation introduced by *Craig* [1961] to describe the relative abundance of heavy ($^1\text{H}_2\text{ }^{18}\text{O}$ and $^1\text{H}^2\text{H}^{16}\text{O}$) water stable isotopes relative to the abundance of light ($\text{H}_2\text{ }^{16}\text{O}$) water stable isotopes

$$\delta^* = (R_{\text{sample}}/R_{\text{VSMOW}} - 1) \times 1000 ,$$

where δ^* represents either $\delta^{18}\text{O}$ or δD and R_{sample} and R_{VSMOW} are the isotopic ratio of the sample and Vienna standard mean ocean water (VSMOW) for the respective isotopic species.

The water stable isotopic composition of precipitation and vapor from an air mass represents an integrative tracer for the hydrological processes that the air mass has undergone. As these processes are affected by climate change, this forms the basis for paleoclimate reconstructions based on records of past precipitation isotopic composition from, for example, ice cores [*European Project for Ice Coring in Antarctica Community Members*, 2006; *North Greenland Ice-Core Project Members*, 2004], calcite [*Wang et al.*, 2008; *Cruz et al.*, 2005], or cellulose records [*Treydte et al.*, 2007]. However, accurate past climate reconstruction requires an ability to understand and quantify how weather and climate is recorded in the stable water isotopes record today and in the past. These issues have been explored using spatial or present-day temporal calibrations, as well as using isotopically enabled atmospheric general circulation models run under different climate states, e.g., for the previous interglacial [*Masson-Delmotte et al.*, 2011; *Sime et al.*, 2013], the Last Glacial Maximum [*Lee et al.*, 2008], for the glacial-interglacial transition [*Schoenemann et al.*, 2014], and for the Holocene [*LeGrande and Schmidt*, 2009]. To allow a robust comparison between ice core records and isotope-enabled simulations, the validity of the representation of water stable isotope in these models therefore needs to be demonstrated.

Here we focus on Greenland, where well-dated, high-resolution ice core records provide accurate information on spatiotemporal variations in water stable isotopes during the recent glacial-interglacial transition [*Steffensen et al.*, 2008]. This focus on Greenland is also motivated by the fact that moisture transport toward the ice sheet is key for the ice sheet mass balance and its global impacts [*Vernon et al.*, 2013; *Hanna et al.*, 2013; *Schoenemann and Cassano*, 2009]. Finally, it is also justified by the control of large-scale atmospheric circulation on moisture transport, through weather regimes and the North Atlantic Oscillation [*Ortega et al.*, 2015; *Merz et al.*, 2013]. As these large-scale atmospheric circulation features are well captured by atmospheric reanalyses, simulations performed with atmospheric models that are equipped with water stable isotopes and nudged to reanalyses can provide a framework to test the capacity of the isotope-enabled simulations.

We now briefly summarize the state-of-the-art for evaluating the performance of isotopic atmospheric models for Greenland. Note that most studies using ice core records have ignored postdeposition effects (e.g., wind scouring and snow metamorphism) and directly compared the simulated precipitation-weighted isotopic composition with seasonal or annual ice core signals.

Several studies have documented systematic biases in the simulated mean annual precipitation-weighted $\delta^{18}\text{O}$ against ice core mean records. Such biases have been shown evidence of using both nudged and free running general circulation models (GCMs) and nudged RCMs [*Werner et al.*, 2001; *Sjolte et al.*, 2011; *Steen-Larsen et al.*, 2011]. Using isotope-enabled GCMs nudged to reanalysis products, e.g., ERA-Interim [*Dee et al.*, 2011], it is possible to compare simulated interannual variation directly with the observed variability (e.g., from ice core and precipitation monitoring data) [*Steen-Larsen et al.*, 2011; *Masson-Delmotte et al.*, 2015a]. The ability to capture the mean value and the interannual variability of $\delta^{18}\text{O}$ (including the recent increasing trend in northwest Greenland) was shown to depend both on the model and on the reanalyses and nudging methods [*Masson-Delmotte et al.*, 2015a].

We now focus on the second-order deuterium excess parameter ($d\text{-excess} = \delta\text{D} - 8 \times \delta^{18}\text{O}$) [*Dansgaard*, 1964]. Using direct water vapor isotope observations from different locations along one remarkable extratropical atmospheric river event, *Bonne et al.* [2015] recently showed that moisture source $d\text{-excess}$ appears to be conserved during atmospheric transport. The theoretical assumption that source $d\text{-excess}$ is influenced by local evaporation conditions [*Merlivat and Jouzel*, 1979] has also been supported by observations, e.g., in the Arctic [*Kurita*, 2011], in the tempered North Atlantic [*Steen-Larsen et al.*, 2015], in the western subtropical North Atlantic [*Steen-Larsen et al.*, 2014b], and eastern tropical North Atlantic [*Benetti et al.*, 2014], and in simulations [e.g., *Jouzel et al.*, 2013]. These lines of evidence support the interpretation of Greenland $d\text{-excess}$ records in terms of changes of evaporation conditions, including marine boundary layer characteristics.

While such features also arise from conceptual models [e.g., *Johnsen et al.*, 1989; *Masson-Delmotte et al.*, 2005; *Uemura et al.*, 2012], the ability of isotope-enabled GCMs to correctly represent Greenland d-excess has only been partly assessed.

Using the ECHAM5-wiso and LMDZiso model nudged to respectively ERA-Interim [*Dee et al.*, 2011] and National Centers for Environmental Prediction (NCEP)-20CR [*Compo et al.*, 2011] reanalysis product *Masson-Delmotte et al.* [2015a] showed that better agreement existed between simulated mean annual precipitation-weighted $\delta^{18}\text{O}$ and observations in northwest Greenland than for the d-excess mean value and variability. It was also shown that the simulation was sensitive to the choice of the reanalysis product [*Masson-Delmotte et al.*, 2015a; *Steen-Larsen et al.*, 2011].

Moreover, recent parallel summer observations of vapor and snow surface isotopes in both Greenland and Antarctica have shown evidence of air-snow vapor exchanges and alteration of the initial snowfall isotope signal in-between successive precipitation events [*Steen-Larsen et al.*, 2014a, 2013; *Ritter et al.*, 2016]. This challenges the classical comparison of simulated precipitation-weighted isotopes directly with ice core isotope records. Here we circumvent this source of uncertainty as well as the averaging process inherent to the ice core signals by comparing model outputs with direct observations of surface water vapor isotopes. Atmospheric water vapor observations with hourly resolution indeed permit model-data comparison at the weather scale. We do not expect the local evaporation to significantly influence the synoptically driven water vapor isotopes due to difference in magnitude of signal.

Early water vapor isotope observations were restricted by the effort needed to collect and measure samples. This involved cold-trap sampling for subsequent laboratory measurement using isotope ratio mass spectrometry. Thanks to the development of commercial water vapor isotope laser spectrometers in the 2000s, it is now possible to accurately and precisely measure in situ the water vapor isotopic composition with a temporal resolution of a few minutes [*Crosson et al.*, 2002; *Baer et al.*, 2002]. The development of robust calibration systems and protocols has further provided calibrated data sets processed at 10 min resolution, reaching respective accuracy and precision for $\delta^{18}\text{O}$, δD , and d-excess of 0.23‰, 1.4‰, and 2.3‰ in Greenland [*Steen-Larsen et al.*, 2013], and approximately twice the accuracy in the subtropics [*Steen-Larsen et al.*, 2014b]. Moreover, autonomous operation can be achieved for weeks to months using custom made calibration systems [*Bailey et al.*, 2015; *Steen-Larsen et al.*, 2014b].

Emerging studies have used such new vapor isotopic composition data for comparison with outputs from isotope-enabled GCMs. Most of these studies used the modeling framework to understand the processes at play. For instance, *Okazaki et al.* [2015] combined the isoGSM model with in situ observations from West Africa to show that upstream precipitation amount is modulating the isotopic signal during the West African monsoon season. *Wei et al.* [2016] quantified the seasonal variability in the fraction of local moisture over a rice paddy in Japan originating from evapotranspiration using combined in situ water vapor isotope observations and simulations from the isoGSM model. For Greenland, *Steen-Larsen et al.* [2013] compared d-excess observations from the NEEM site (above the northwest Greenland ice sheet) with outputs of the LMDZiso model, including water tagging. The model outputs were used to identify the fraction of local moisture with an Arctic origin. The simulated vapor isotopic composition showed systematic biases and had much lower day-to-day variability than observed. The lack of variability in simulated d-excess was also identified in LMDZiso on coastal South Greenland [*Bonne et al.*, 2014]. Interestingly, both the LMDZiso and ECHAM5-wiso models are capable of correctly simulating the low d-excess of moisture transported toward South Greenland and NEEM along an atmospheric river event [*Bonne et al.*, 2015] but do not produce the high d-excess associated with Arctic air masses. These preliminary findings, restricted to a short observation period, motivate systematic model-data comparisons.

The purpose of this paper is therefore to develop methodologies for comparing daily mean observations of atmospheric water vapor isotopes obtained during several summers at the NEEM site with outputs from five different simulations using AGCMs (ECHAM5-wiso, isoGSM, LMDZiso-no_seaice, LMDZiso-seaice, and LMDZiso-no_seaice_zoom, when referring to the combined set of LMDZiso simulation we will refer to simulations simply as “LMDZiso”), nudged to reanalysis products. We have analyzed the ability of these models to capture mean values, as well as day-to-day variability, and characteristics of isotope-humidity relation related to both air mass distillations and changes in moisture origins. This finally motivates a comparison of the mean spatial patterns of North Atlantic/Arctic surface water vapor isotopic composition.

Table 1. Characteristics (Mean Value Over the Observation Period and Associated Standard Deviations) of Observed and Simulated Daily Mean Humidity, $\delta^{18}\text{O}$, d-Excess, and Surface Air Temperature^a

	Observations	ECHAM5-wiso	isoGSM	LMDZiso-no_seaice/seaice	LMDZiso-no_seaice-zoom
Humidity (ppmv)	3900 ± 1400	4000 ± 1200	5200 +/-1500	3600 ± 1000	3100 ± 1000
$\delta^{18}\text{O}$ (‰)	-39.0 ± 4.7	-36.3 ± 4.3	-28.1 ± 3.3	-31.9 ± 2.9	-29.5 ± 2.9
δD (‰)	-286 ± 30	-272 ± 32	-213 ± 24	-240 ± 22	-226 ± 23
d-excess (‰)	26 ± 7	17 ± 4	13 ± 5	15 ± 2	9.7 ± 1.4
Temperature (°C)	-8.4 ± 4.2	-9.0 ± 3.8	-4.9 ± 4.3	-9.4 ± 3.6	-11.0 ± 3.8
Elevation (m.a.s.l)	2480	2340	2000	2300	2500

^aThe bottom line displays the elevation of the NEEM site and the corresponding model grid cell.

This manuscript is organized in the following way. Section 2 describes our observations, the different models, and the simulation setup. Section 3 is devoted to the model-data and model-model comparisons. The discussion of section 4 is focused on model skills and biases, in relation to the role of the initial water vapor isotopic composition in the source region. It also investigates the implications of these errors for the use of these models for ice core data interpretation, and future pathways to better simulate the atmospheric water vapor isotopic composition above and around the Greenland ice sheet. Our key conclusions and recommendations for future work are summarized in section 5.

2. Observation and Simulation Data Sets

2.1. Atmospheric Observations

Atmospheric monitoring was carried out as part of the international deep drilling program at the NEEM site in northwest Greenland (77.45°N, 51.05°W; 2484 m above sea level (asl)) during 178 days across the summer season field campaigns of 2010 (24 May to 3 August), 2011 (5 July to 3 August), and 2012 (21 May to 3 August). Within the framework of the International Polar Year, the international deep drilling at NEEM was initiated in 2007. From this project the first Greenland record spanning the previous interglacial period was produced [NEEM Community Members, 2013] as well as a stacked ice core record based on multiple shallow ice cores spanning the past couple of centuries [Masson-Delmotte *et al.*, 2015a]. As part of the NEEM surface program in addition to surface air temperature measurements, water vapor isotope observations (including humidity) were performed using either a Los Gatos Research Inc. ICOS-analyzer (2010 season) or a Picarro Inc. CRDS-analyzer (2011 and 2012 season). The water vapor isotopic composition was measured at 1 m (2010 season) and at 3 m (2011 and 2012 season) above the snow surface. We only observed differences between measurements at these different heights during diurnal variations and did not identify systematic differences for daily average values [Steen-Larsen *et al.*, 2013]. The reader is referred to the original publications of our data sets (temperature, humidity, and water vapor isotope data) for detailed descriptions of the measurement and calibration protocols [Steen-Larsen *et al.*, 2014a, 2013], and the reader is referred to these papers for details on measurements and calibration protocol. The estimated uncertainty on $\delta^{18}\text{O}$, δD , and d-excess is ~0.23‰, 1.4‰, 2.3‰, respectively [Steen-Larsen *et al.*, 2013].

Altogether, the multisummer mean values for temperature, humidity, $\delta^{18}\text{O}$, δD , and d-excess at NEEM are of -8.3°C, 3500 ppmv, -39‰, -286‰, and 26‰, respectively (Tables 1 and S1 in the supporting information). Average seasonal temperature and humidity mean values vary between -9.5 and -6.8°C, and 3200 to 4500 ppmv. We note that the warmest and wettest season is observed in 2011 because our shorter measurement campaign only occurred during the middle of the summer.

Daily mean $\delta^{18}\text{O}$ and δD vary between -52‰ and -27‰ for $\delta^{18}\text{O}$, and between -393‰ and -202‰ for δD . Seasonal mean values range from -40.5‰ to -38.0‰ for $\delta^{18}\text{O}$ and -294‰ to -281‰ for δD . Large variations occur in daily mean d-excess values, from 12‰ to 52‰, with large interdaily variations during summer 2010. However, seasonal mean values only vary between 23‰ and 29‰.

In the model-data comparison, we will also use mean summer values of isotopic composition from three sites in the North Atlantic marine boundary layer: Bermuda Islands (32.26°N, 64.88°W) [Steen-Larsen *et al.*, 2014b], Iceland (63.83°N, 21.47°W) [Steen-Larsen *et al.*, 2015], and unpublished recent data from Svalbard (78.93°N, 11.03°E) [Masson-Delmotte *et al.*, 2015b]. Measurements carried out at these stations have all been calibrated

using standards referenced against the international VSMOW-SLAP scale using protocols described in [Steen-Larsen *et al.*, 2014b].

2.2. Model Description and Simulation Setup

In this paper, we use outputs from five different simulations carried out using three different atmosphere-only GCMs. We first describe the different model resolutions. ECHAM5-wiso [Werner *et al.*, 2011] is run at T106L31 resolution corresponding to approximately $1.125^\circ \times 1.125^\circ$ horizontal grid size and 31 vertical levels. IsoGSM [Yoshimura *et al.*, 2008] is run in T63L28 resolution corresponding to approximately $1.875^\circ \times 1.875^\circ$ horizontal grid size and 28 vertical levels. LMDZ4iso [Risi *et al.*, 2010] is run in two different resolution configurations. The first one (referred hereafter as LMDZiso-no_seaice and LMDZiso-seaice) has a spatial resolution of 2.5° (latitude) by 3.75° (longitude) and 39 vertical levels. The second configuration (referred hereafter as LMDZiso-no_seaice-zoom) has a zoomed grid centered on the North Pole allowing a higher latitudinal resolution between 65° and 90°N (0.37°), but a reduced resolution at lower latitudes (1.1° at 40°N , and 2.5° at 25°N). Also, in the zoom version the longitudinal resolution is 3.75° . For the different model simulations the top of the lowest grid level is about 25–35 m for representative locations in the subtropical Atlantic. Typically for the different model setups the number of grid boxes in the subtropical oceanic planetary boundary level varies between 7 and 11.

Hereafter, we use model outputs at the grid point encompassing the NEEM camp with a true elevation of 2480 m asl. The model simulation grid point elevation is 2340 m asl, for ECHAM5wiso, 2000 m for isoGSM, 2300 m for LMDZiso-no_seaice/seaice, and finally 2500 m for LMDZiso-no_seaice-zoom (Table 1). These differences have implications for simulated temperature, moisture transport, and isotopic distillation. We note that the used simulated water vapor isotopic value is the mean of the lowest grid cell, while the measured water vapor isotopic composition is measured at 1 and 3 m above the snow surface. This difference in elevation between measured and simulated isotopes will have a significant influence on the diurnal variability, but we do not expect a significant influence on the synoptic variability.

We now describe the different nudging techniques. ECHAM5-wiso is run nudged to the wind, temperature, and surface pressure fields from ERA-Interim [Dee *et al.*, 2011]. IsoGSM is run nudged to wind and temperature fields from NCEP-DOE R2 [Kanamitsu *et al.*, 2002]. All of the LMDZiso simulations are nudged only to the wind field from the ECMWF-operational analysis.

Different initializations of ocean surface isotopic composition are also implemented. ECHAM5-wiso uses the global seawater $\delta^{18}\text{O}$ database version 1.1 [LeGrande and Schmidt, 2006] and assumes a seawater d-excess of zero, while isoGSM is prescribed a homogeneous ocean surface isotopic composition of 0‰ globally. LMDZiso simulations are prescribed a homogeneous ocean surface isotopic composition (0.5‰ and 4.0‰ for $\delta^{18}\text{O}$ and δD , respectively).

Finally, sea ice and sea surface temperature (SST) are provided by ERA-Interim for ECHAM5-wiso and by the NCEP reanalysis for isoGSM. SST is prescribed by the NCEP reanalysis for LMDZiso. Sea ice is prescribed for LMDZiso in two different configurations. For LMDZiso-no_seaice and LMDZiso-no_seaice-zoom no sea ice exists once the surface temperature of the Arctic is above -1.8°C . This means that there is no sea ice coverage in the Arctic during June–August. For the LMDZiso-seaice simulation the extent of the sea ice is equivalent with sea ice extent in ECHAM5-wiso.

Of course, differences between the simulations will also arise from the differences in the atmospheric model themselves, especially the model physical parameterizations affecting the water cycle, and from differences in the implementation of water stable isotopes. The reader is referred to the initial model description papers for details on the water isotope implementation. In all these models, isotopic fractionation associated with ocean evaporation is parameterized as in Merlivat and Jouzel [1979], and isotopic fractionation during snow crystal formation is also systematically prescribed following Jouzel and Merlivat [1984], albeit with differences in the parameterization of the supersaturation dependency on temperature. LMDZiso is using the function $S = 1.0 - 0.004 T$. The fractionation coefficient is implemented in ECHAM5-wiso and isoGSM as a linear interpolation between that of ice and that of water for temperatures above -35°C (ECHAM5-wiso) and -20°C (isoGSM). For ECHAM5-wiso below -35°C , the supersaturation function $S = 1.0 - 0.004 T$ is used, while for isoGSM, below -20°C , the supersaturation function $S = 1.0 - 0.003 T$ is used. We note that nudging differences for the different simulations also constitute an impediment to the individual model versus data evaluation.

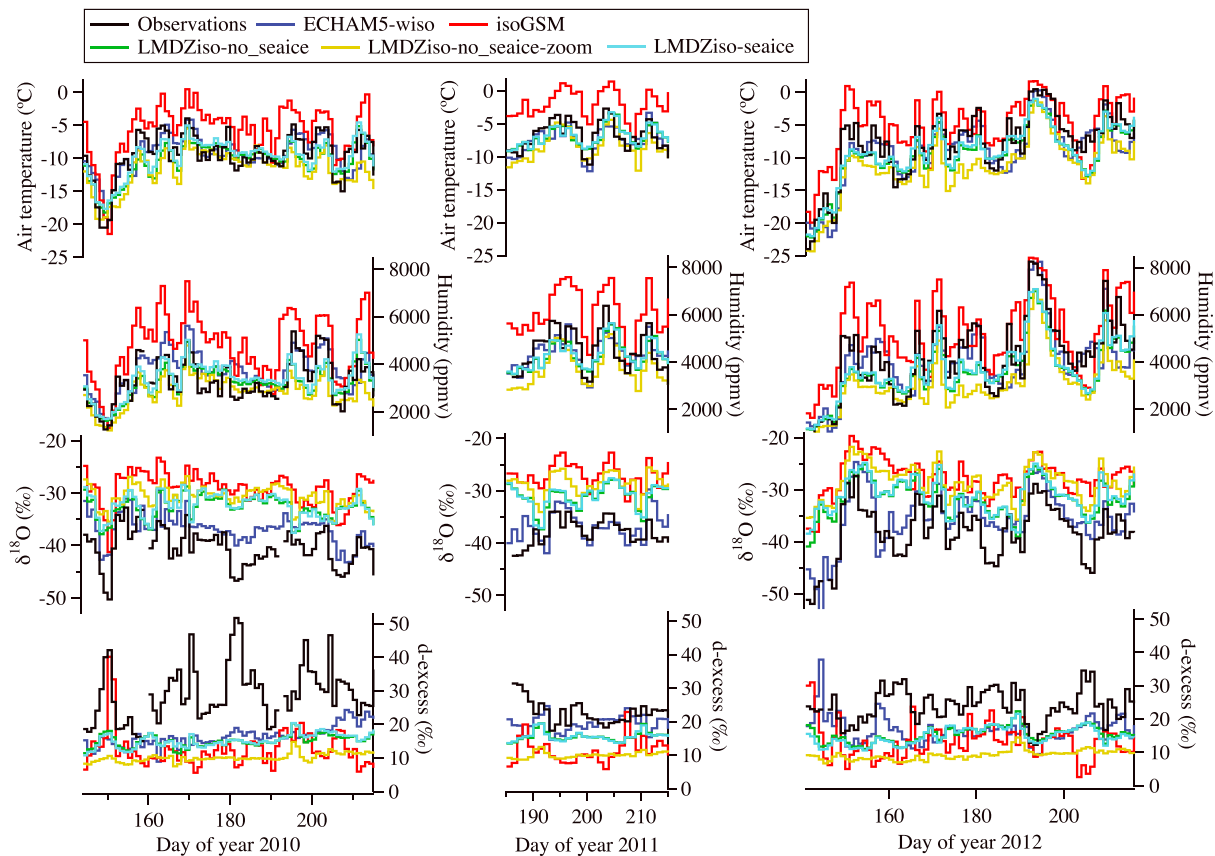


Figure 1. Daily observed (black) and simulated values at NEEM of surface (2 m) air temperature (°C), humidity (ppmv), $\delta^{18}\text{O}$, and d-excess (‰) (blue, ECHAM5-wiso; red, isoGSM; green, LMDZiso-no_seaice; light blue, LMDZiso-seaice; and dark yellow, LMDZiso-no_seaice-zoom) for 2010 (left column), 2011 (middle column), and 2012 (right column).

However, we expect this to only be a minor effect. We refer the reader to *Yoshimura and Kanamitsu [2008]* for a discussion of the influence on the modeling skills by nudging technique.

We note that these models have crude representations of snow-atmosphere exchanges. For this purpose, we do not compare their results with our observations at the subdiurnal scale and focus on daily average values.

3. Results

3.1. NEEM Model-Data Comparisons

Figure 1 displays the various model outputs with our daily observations for the three seasons 2010, 2011, and 2012. To varying degrees, the models capture part of the observed day-to-day variability in temperature, humidity, and $\delta^{18}\text{O}$ but fail to reproduce the observed variations in d-excess.

In order to better quantify systematic biases in the models, we have reported the average observed and simulated values in Tables 1 and Figure S1. First, we note that the simulation using LMDZiso-no_seaice and LMDZiso-seaice results in the same temperature, humidity, and isotopic variation at the NEEM site on top of the Greenland Ice Sheet (notice that the lines are on top of each other in Figure 1). Second, we note that the range of simulated temperature and humidity in ECHAM5-wiso and LMDZiso is compatible with NEEM observations. We identify a warm and moist bias for isoGSM, consistent with a lower local elevation (Table 1). All models underestimate the isotopic depletion at NEEM and produce too enriched $\delta^{18}\text{O}$ as well as too low d-excess levels. Surprisingly, LMDZiso-no_seaice-zoom deviates more from the NEEM observations than LMDZiso-no_seaice/seaice, as it produces colder and drier conditions, but lower (−6‰) d-excess and more enriched (+2.5‰) $\delta^{18}\text{O}$ values, compared to LMDZiso-no_seaice/seaice. In this case, the zoom version with higher spatial resolution leads to larger errors in the model simulation of stable water isotopes above NEEM.

The characteristics of humidity and temperature of all simulations align on the Clausius-Clapeyron relationship (supporting information Figure S5). This emphasizes the strong control of the simulated temperature on the simulated humidity.

Figure 1 shows a coherent pattern between the individual simulations of the day-to-day variability for temperature and humidity, as expected from the fact that each simulation is nudged to reanalysis products. However, this is not the case for the simulations of the water vapor isotopic composition. It is particularly obvious when comparing the same model, but with different spatial resolution (LMDZiso-no_seaice/seaice and LMDZiso-no_seaice-zoom). This shows that each simulation differs in the transport of moisture, and/or in the isotopic composition of moisture from different sources and suggests that evaluating the model-data agreement using water isotopes may provide additional insight.

In order to provide quantitative information on skills of the models in simulating the day-to-day isotopic variability, we now employ the classical Taylor diagrams [Taylor, 2001], developed for model evaluation and model-intercomparisons (Figure 2) and investigate the linear relationships between model outputs and observations (Table 2).

All models have good skills for air temperature day-to-day variability ($R > 0.82$) and humidity ($R > 0.79$). The warm bias of isoGSM appears even more strongly as a wet bias, coherent with the exponential shape of the Clausius-Clapeyron relationship (Figure 2b, red circle). Similarly, the cold bias of LMDZiso-no_seaice-zoom results in a reduced skill for humidity compared to its skill for temperature.

The different simulations rely on different nudging methodologies. Surprisingly, even though LMDZiso simulations are only nudged to large-scale winds, they have similar skills for air temperature and humidity as ECHAM5-wiso and isoGSM, which are also nudged to temperature.

While ECHAM5-wiso produces rather similar skills for $\delta^{18}\text{O}$ and for humidity, this is not the case for isoGSM and LMDZiso, which all have lower performance for $\delta^{18}\text{O}$. We note that the zoom version of LMDZiso produces better results for $\delta^{18}\text{O}$ day-to-day variability, despite larger systematic biases.

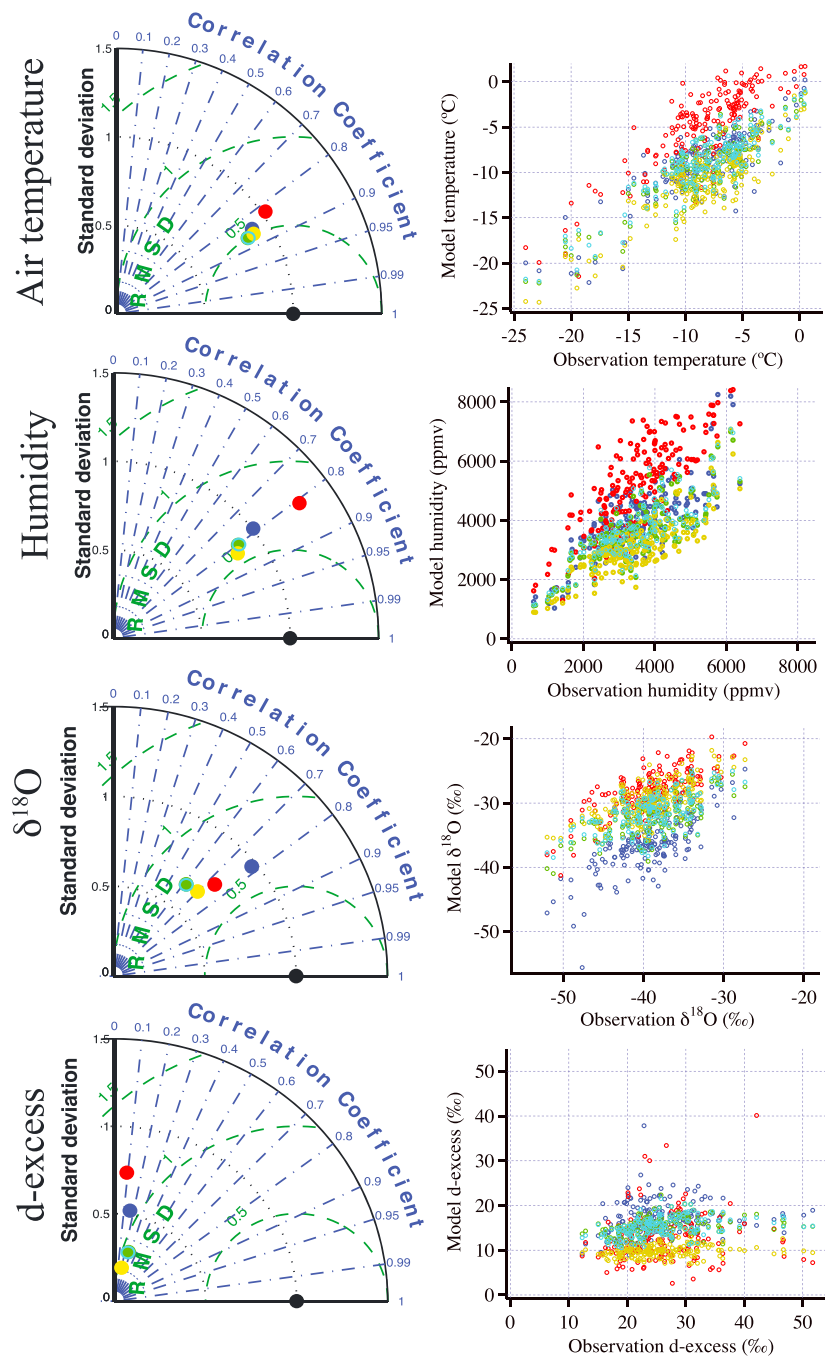
Finally, the model skills for d-excess are poor, with correlation coefficients ranging from about 0.1 to 0.3. While LMDZiso produce the smallest day-to-day d-excess variability, these simulations show some correlation with the observed d-excess variability ($R = 0.2$ to 0.3), while the other models fail to achieve this. Puzzlingly, the zoom version seems to improve the LMDZiso model skill for $\delta^{18}\text{O}$ but degrades it for d-excess.

We have also investigated the model skills for each summer season. Due to the occurrence of several extratropical storms during summer 2012, including a remarkable atmospheric river event, which was an event that brought a large amount of moisture through a narrow corridor from the subtropics and to the Greenland Ice Sheet [Bonne *et al.*, 2015], all models show the best skills in simulating the observed $\delta^{18}\text{O}$ and d-excess during this 2012 season (Figure S1 in supporting information). This implies that the transport of moisture along the North Atlantic and the isotopic characteristics of the initial vapor formed in the North Atlantic subtropics are correctly captured by all models.

3.2. Comparison With Other North Atlantic Sites

Figure 3 shows the observed versus simulated relationship between $\delta^{18}\text{O}$ and humidity for the NEEEM site, as well as for three marine boundary layer sites in the North Atlantic (Bermuda, Iceland, and Svalbard). The data depict an enhanced slope for NEEEM, a feature expected both from a Rayleigh distillation and from a mixing process (Figure 3). A mixing line (the line formed in a $\delta^{18}\text{O}$ -humidity plot, when mixing with varying degree two different end-members of distinct $\delta^{18}\text{O}$ and humidity value) and a Rayleigh distillation line starting from Bermuda (the line formed in a $\delta^{18}\text{O}$ -humidity plot, when an air parcel is distilled continuously and the condensate is removed immediately) is shown in the figure.

NEEM observations depict a close relationship between $\delta^{18}\text{O}$ and humidity ($R = 0.7$), with a steep slope. Models generally underestimate the strength of the correlation, with the exception of isoGSM, which may be related to its wet bias and larger simulated humidity variability. All but ECHAM5-wiso severely underestimate the $\delta^{18}\text{O}$ -humidity slope (Table 3 and Figure 4). When comparing the different sites, it appears that LMDZiso-no_seaice and LMDZiso-no_seaice-zoom tend to produce a pattern for Svalbard, which is closer



● Observations ● LMDZiso-no_seaice ● LMDZiso-seaice
 ● ECHAM5-wiso ● isoGSM ● LMDZiso-no_seaice-zoom

Figure 2. Taylor diagrams showing the normalized standard deviation and the correlation coefficient of each simulation output (color) with the observations (black) for different variables at NEEM (from top to bottom: air temperature, humidity, $\delta^{18}\text{O}$, and d-excess). The right panels depict the direct comparison of model outputs (y axis) against observations (x axis) for each variable, using the data sets for all three seasons.

to the theoretical mixing line than the Rayleigh distillation line. However, for the LMDZiso_seaice simulation the pattern for Svalbard is closer to the Rayleigh distillation line, which illustrates the influence of the sea ice extent on the air mass mixing in the Arctic perhaps resulting in a decrease exchange between the atmosphere and the ocean.

Table 2. Linear Analysis of Relationships Between Simulations and Observations (Slope and Correlation Coefficients, R) Calculated Using the Whole Data Set (187 Daily Mean Values Over Three Seasons)^a

	ECHAM5-wiso	isoGSM	LMDZiso-no_seaice/seaice	LMDZiso-no_seaice-zoom
Temperature	0.77 ± 0.04 $R = 0.85 \pm 0.04$	0.84 ± 0.04 $R = 0.82 \pm 0.04$	0.74 ± 0.03 $R = 0.87 \pm 0.04$	0.77 ± 0.03 $R = 0.86 \pm 0.04$
Humidity	0.71 ± 0.05 $R = 0.83 \pm 0.05$	0.89 ± 0.05 $R = 0.83 \pm 0.05$	0.62 ± 0.03 $R = 0.81 \pm 0.05$	0.60 ± 0.03 $R = 0.83 \pm 0.04$
$\delta^{18}\text{O}$	0.76 ± 0.05 $R = 0.78 \pm 0.05$	0.55 ± 0.04 $R = 0.74 \pm 0.05$	0.40 ± 0.04 $R = 0.61 \pm 0.06$	0.46 ± 0.04 $R = 0.70 \pm 0.05$
δD	0.82 ± 0.04 $R = 0.81 \pm 0.04$	0.57 ± 0.04 $R = 0.76 \pm 0.05$	0.42 ± 0.04 $R = 0.62 \pm 0.06$	0.49 ± 0.04 $R = 0.70 \pm 0.05$
d-excess	<i>0.09 ± 0.04</i> $R = 0.16 \pm 0.08$	<i>0.07 ± 0.06</i> $R = 0.09 \pm 0.08$	<i>0.08 ± 0.02</i> $R = 0.27 \pm 0.07$	<i>0.04 ± 0.015</i> $R = 0.19 \pm 0.07$

^aNotice that the calculated slopes for the d-excess is not significant as determined using an F test at the 95% confidence level (marked with italic). The uncertainty on the slope represents the standard deviation and the uncertainty on the correlation coefficient represents the standard error.

We now explore the relationships between d-excess and $\delta^{18}\text{O}$ (Figure 4 and Table 3). Despite its warm and wet bias, and its mismatch for the slope between $\delta^{18}\text{O}$ and humidity, isoGSM is the only model able to capture the observed d-excess versus $\delta^{18}\text{O}$ relationship. All other models strongly underestimate the slope of the relationship between d-excess on $\delta^{18}\text{O}$. For the LMDZiso-no_seaice-zoom model the d-excess versus $\delta^{18}\text{O}$ slope is about half of the slope for LMDZiso-no_seaice/seaice.

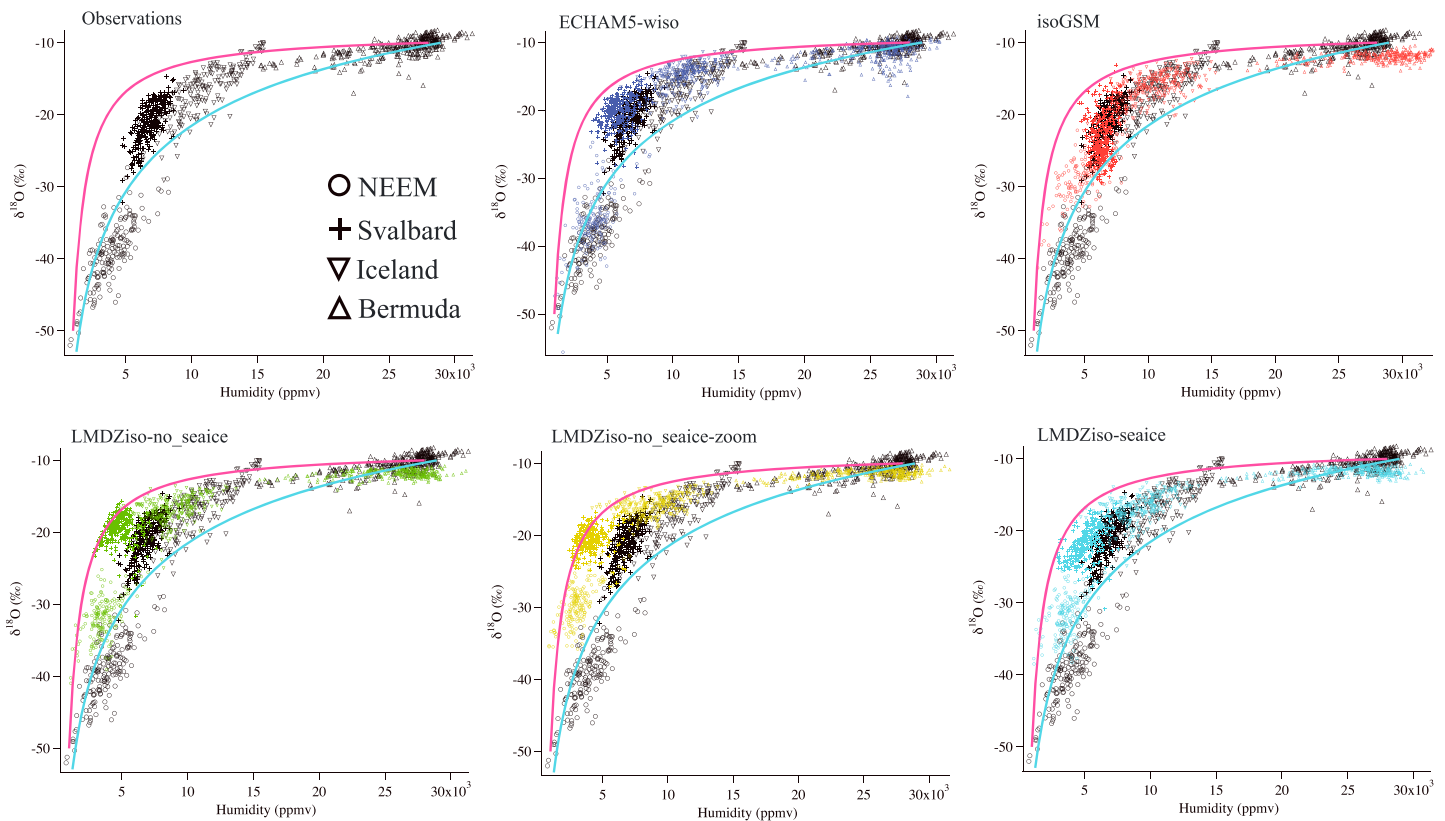


Figure 3. Observed (upper left) and simulated relationships between $\delta^{18}\text{O}$ and humidity for Bermuda (triangles), Iceland (inverted triangles), Svalbard (crosses), and NEEM (open circles). In all panels, the cyan solid line represents the same theoretical calculation of a Rayleigh distillation model starting from the observed Bermuda data and the red solid line represents a theoretical mixing line between two observed end-members (Bermuda and NEEM).

Table 3. Linear Regression Results (Slope and Correlation Coefficients, R) for Observed and Simulated Relationships Between $\delta^{18}\text{O}$ and Temperature, $\delta^{18}\text{O}$ and Humidity, and d-Excess Versus $\delta^{18}\text{O}$ at NEEM (Figure 4)^a

Slope All Data	Observations	ECHAM5-wiso	isoGSM	LMDZiso-no_seaice/seaice	LMDZiso-no_seaice-zoom
$\delta^{18}\text{O}$ versus temperature	0.82 ± 0.05 $R = 0.78 \pm 0.05$	0.73 ± 0.06 $R = 0.65 \pm 0.06$	0.54 ± 0.04 $R = 0.70 \pm 0.05$	0.43 ± 0.05 $R = 0.55 \pm 0.06$	0.44 ± 0.05 $R = 0.57 \pm 0.06$
$\delta^{18}\text{O}$ versus humidity	$2.5e-3 \pm 0.2e-3$ $R = 0.77 \pm 0.05$	$2.3e-3 \pm 0.2e-3$ $R = 0.61 \pm 0.06$	$1.59e-3 \pm 0.12e-3$ $R = 0.71 \pm 0.05$	$1.6e-3 \pm 0.2e-3$ $R = 0.55 \pm 0.06$	$1.7e-3 \pm 0.2e-3$ $R = 0.59 \pm 0.06$
d-excess versus $\delta^{18}\text{O}$	-0.99 ± 0.09 $R = -0.64 \pm 0.06$	-0.64 ± 0.04 $R = -0.77 \pm 0.05$	-0.99 ± 0.09 $R = -0.64 \pm 0.06$	-0.49 ± 0.04 $R = -0.71 \pm 0.05$	-0.22 ± 0.03 $R = -0.48 \pm 0.07$

^aThe uncertainty on the slope represents the standard deviation and the uncertainty on the correlation coefficient represents the standard error.

We further investigate now the differences between the two spatial resolution LMDZiso simulations (no_seaice/seaice versus no_seaice-zoom simulations) (Figure S2 and Table S2 in the supporting information). We observe that these simulations produce high correlation between their simulation outputs of temperature ($R=0.99$), humidity ($R=0.90$), and $\delta^{18}\text{O}$ ($R=0.88$), but major differences for d-excess ($R=0.47$). It can be noted that the d-excess versus $\delta^{18}\text{O}$ relationship of LMDZiso-no_seaice-zoom deviates more from the observed one than that of LMDZiso-no_seaice/seaice. This strengthens the earlier seemingly puzzling conclusions that the enhanced resolution tends to increase the LMDZiso model biases for water isotopes.

We finally explore whether model biases at the NEEM site may result from model biases in simulating the initial vapor isotopic composition in the marine boundary layer. For this purpose, we compare the simulated spatial distribution of $\delta^{18}\text{O}$ and d-excess in the lowest model layer in the North Atlantic sector (Figure 5). As expected from their similar representation of evaporation fractionation processes, all models produce similar spatial patterns in the North Atlantic. However, large intermodel differences appear in the Baffin Bay region, Canadian Arctic, and the Arctic Ocean. Locally, the intermodel spread can reach up to 3000 ppmv for humidity, 8‰ for $\delta^{18}\text{O}$, and 10‰ for d-excess (Figure S3). We show in the supporting information (Figure S4) the mean June–August (JJA) sea ice cover for isoGSM and ECHAM5-wiso (LMDZiso-seaice uses the same sea ice extent as ECHAM5-wiso).

When compared with the “climatological” JJA average from in situ measurements, available from Bermuda, Iceland, South Greenland (Ivittuut), and Svalbard, we note that all models tend to underestimate (too depleted) the $\delta^{18}\text{O}$ level in Bermuda but produce results consistent with observations for Iceland. A group of three models (ECHAM5wiso, LMDZiso_no_seaice, and LMDZiso-no_seaice-zoom) produce too enriched values in South Greenland and Svalbard. This seems to arise from their simulated enriched $\delta^{18}\text{O}$ values in Baffin Bay and in the Arctic regions (Figures 6 and S3). By contrast, isoGSM and LMDZiso-seaice produces relatively depleted surface $\delta^{18}\text{O}$ levels in the Arctic and Svalbard. These results imply that (i) model biases for NEEM are not representative of Arctic surface vapor results; (ii) there is no robust multimodel pattern in Arctic surface vapor $\delta^{18}\text{O}$, and results are highly model dependent; (iii) models fail to correctly simulate the latitudinal gradient in surface vapor $\delta^{18}\text{O}$. The enriched bias in Greenland and North Atlantic seems to be part of a general hemispherical problem as documented by *Risi et al.* [2012] based on satellite observations and simulations from the SWING2 model intercomparison exercise.

The d-excess observations show a positive meridional surface vapor d-excess gradient, with lower values in Bermuda, and increasing high values toward the Arctic. This compilation confirms the hypothesis of *Steen-Larsen et al.* [2013] and *Steen-Larsen et al.* [2015], purely based on NEEM data and observations from Iceland and South Greenland projected on the origin of corresponding air mass trajectories, and the work of *Kurita* [2011]. This northward d-excess increase is not captured by any of the simulations, which tend to produce low values in the Greenland Sea. Again, isoGSM and LMDZiso-seaice produces high d-excess values for the Canadian Arctic and Arctic Ocean, possibly coupled to the low $\delta^{18}\text{O}$ values and intense distillation. This analysis suggests that the model biases at NEEM for d-excess likely result from model biases in the representation of the marine boundary layer d-excess, especially in areas such as the Baffin Bay and the Arctic region around Greenland.

○ Observations ○ ECHAM5-wiso ○ isoGSM
○ LMDZiso-no_seaice ○ LMDZiso-seaice
○ LMDZiso-no_seaice-zoom

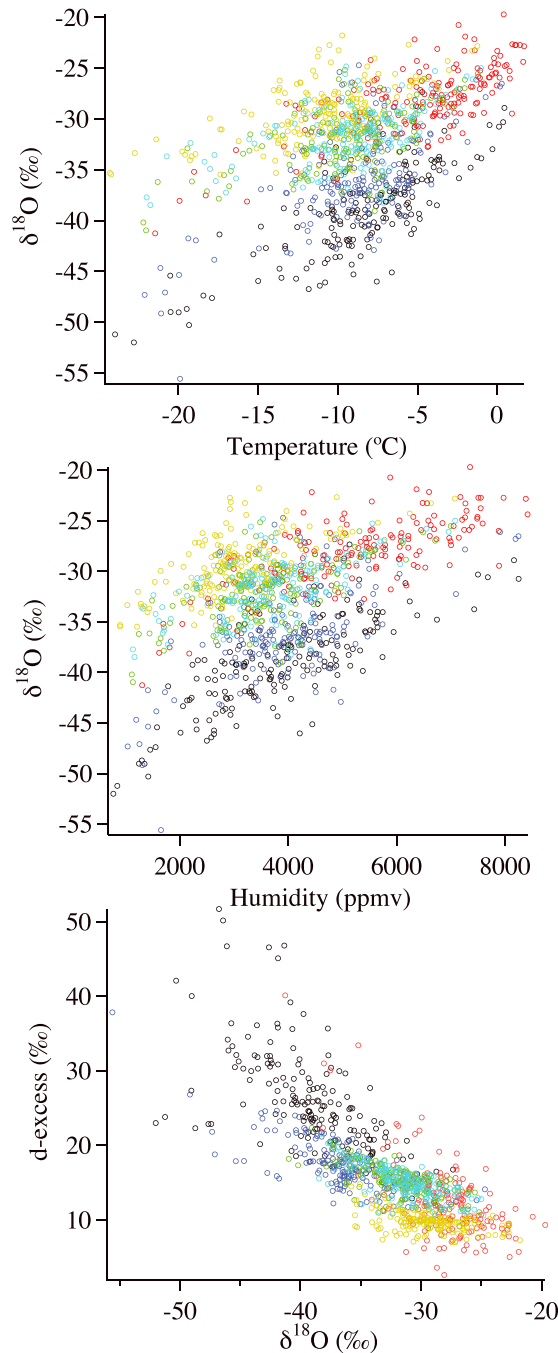


Figure 4. Observed (black) and simulated (colors) relationships between NEEM $\delta^{18}\text{O}$ and temperature (top), NEEM $\delta^{18}\text{O}$ and humidity (middle), and NEEM d-excess versus $\delta^{18}\text{O}$ (bottom). Linear regression results are displayed in Table 3.

vapor observations. This finding is consistent with earlier studies reporting a positive bias when comparing precipitation isotopic composition with Greenland ice core data [Steen-Larsen *et al.*, 2011; Sjolte *et al.*, 2011; Masson-Delmotte *et al.*, 2015a]. Our intercomparison of model biases for vapor $\delta^{18}\text{O}$ shows that they cannot

4. Discussion

4.1. Model Performance for Temperature and Humidity

Some of the simulation biases likely arise from differences in surface elevation at the NEEM location (and possibly also from the shape of the ice sheet), such as the different temperature biases in LMDZiso or the warm bias of isoGSM. The ECHAM5-wiso and LMDZiso show a cold bias. This is in contrast to earlier model evaluations for Greenland using different model simulations [Sjolte *et al.*, 2011; Walsh *et al.*, 2008]. This difference could potentially arise because those simulations were not nudged. It is notable that the zoom version of LMDZiso does not improve the model skill for day-to-day temperature variations (supporting information Figure S2 and Table S2).

Across all models, simulated humidity and air temperature are generally related through the Clausius-Clapeyron relationship (Figure S5). Model biases in the humidity could be a result of the simulated bias in the temperature, which in part is controlled by elevation and indirectly the model resolution. Model skill for day-to-day humidity is generally close to that for temperature. It is not improved by complex nudging schemes including temperature and surface pressure. When comparing the modeled relative humidity for the different simulations with the observed relative humidity, it is generally observed that for high relative humidity the modeled relative humidity is too low and vice versa (figure not shown). This is consistent with the observation that the slope of the modeled humidity versus observed humidity is less than 1 and smaller than the slope for the modeled temperature versus observed temperature (Figure 2 and Table 2). The model bias in specific humidity is primarily mainly due to the model bias in relative humidity.

4.2. Model Performance for $\delta^{18}\text{O}$

We observe a systematic positive bias of simulated $\delta^{18}\text{O}$ at NEEM against surface

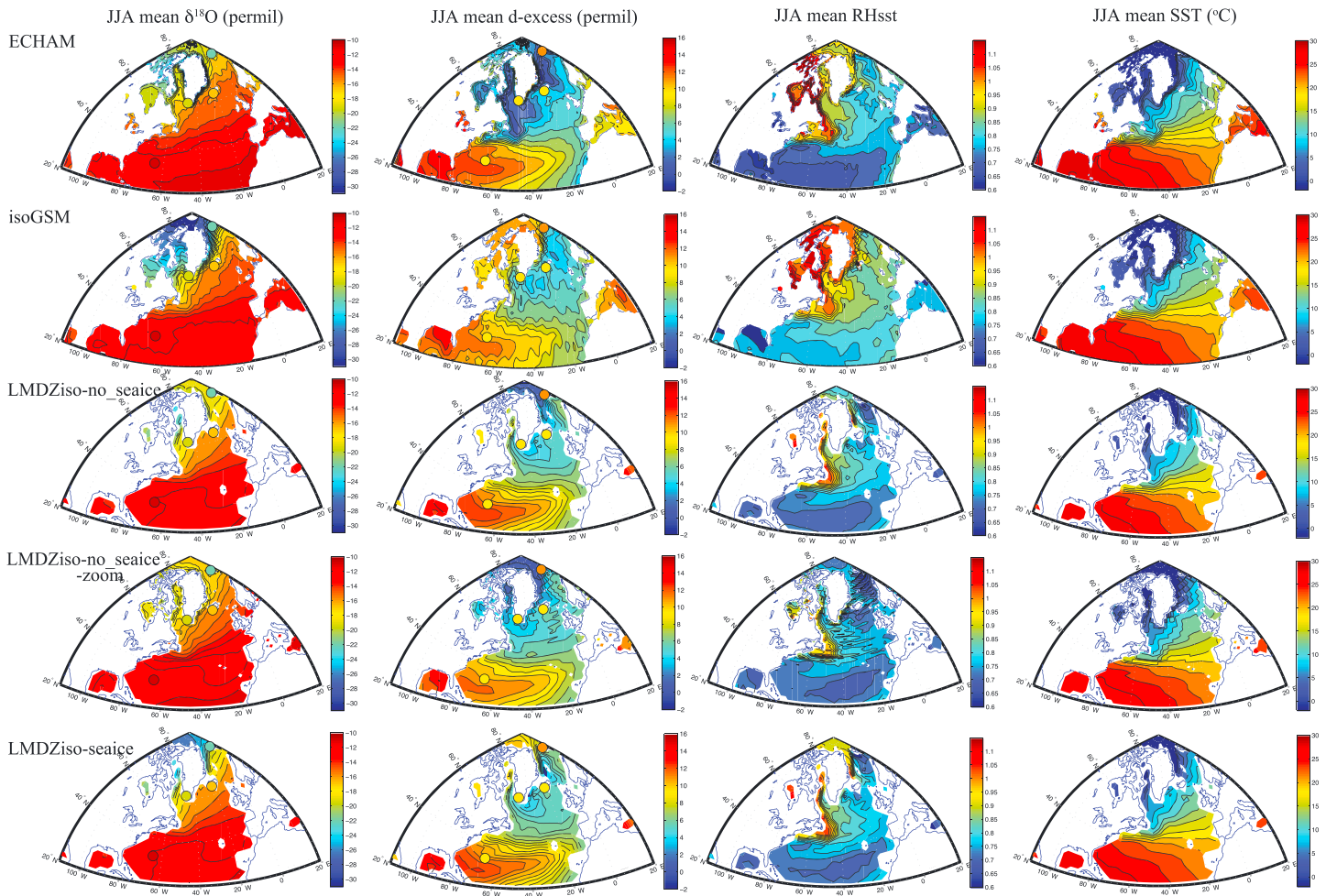


Figure 5. Spatial patterns in the mean JJA surface vapor isotopic composition: from the left $\delta^{18}\text{O}$, d-excess, RHsst, and SST for each model (from the top: ECHAM5wiso, isoGSM, LMDZiso-no_seaice, LMDZiso-no_seaice-zoom, and LMDZiso-seaice). The “climatology” from observations in Bermuda, Iceland, South Greenland, and Svalbard data is displayed as filled circles in each panel.

be simply attributed to temperature or humidity biases: even for a given specific humidity, simulated vapor $\delta^{18}\text{O}$ is more enriched than observed (Figure 4). This challenges the earlier explanations of the enriched bias observed in Greenland ice core data (assuming that vapor $\delta^{18}\text{O}$ is linked with precipitation $\delta^{18}\text{O}$) and rather points to the role of upstream processes.

We first test if the relationship between $\delta^{18}\text{O}$ and humidity simulated for the NEEM site is representative for conditions above the Greenland Ice Sheet. In the supporting information (Figure S6) is shown the distribution of $\delta^{18}\text{O}$ versus humidity for all of the grid cells covering Greenland. We note that the relationship observed for NEEM is consistent with the relationship for the rest of Greenland.

We also notice, based on analysis of spatial patterns that the model biases for NEEM $\delta^{18}\text{O}$ may result either from too enriched $\delta^{18}\text{O}$ in the North Atlantic marine boundary layer vapor, and/or from too low surface humidity values in areas of the North Atlantic and Arctic (Figures 3 and 5). This is supported by coherent inter-model differences in the North Atlantic and for NEEM. For instance, LMDZiso-no_seaice-zoom produces the most enriched $\delta^{18}\text{O}$ in the North Atlantic marine boundary layer, and LMDZiso produce the lowest humidity in the marine boundary layer. As expected from a Rayleigh distillation toward NEEM, they produce more enriched $\delta^{18}\text{O}$ than ECHAM5-wiso, despite similar local humidity levels. Focusing now on LMDZiso (Figure 6), we stress large differences in the simulations of Baffin Bay surface $\delta^{18}\text{O}$ between LMDZiso-no_seaice and LMDZiso-no_seaice-zoom, similar to their offsets at NEEM, coherent with the documentation of storm tracks from this area to NEEM [Steen-Larsen et al., 2011]. Further investigations are required to

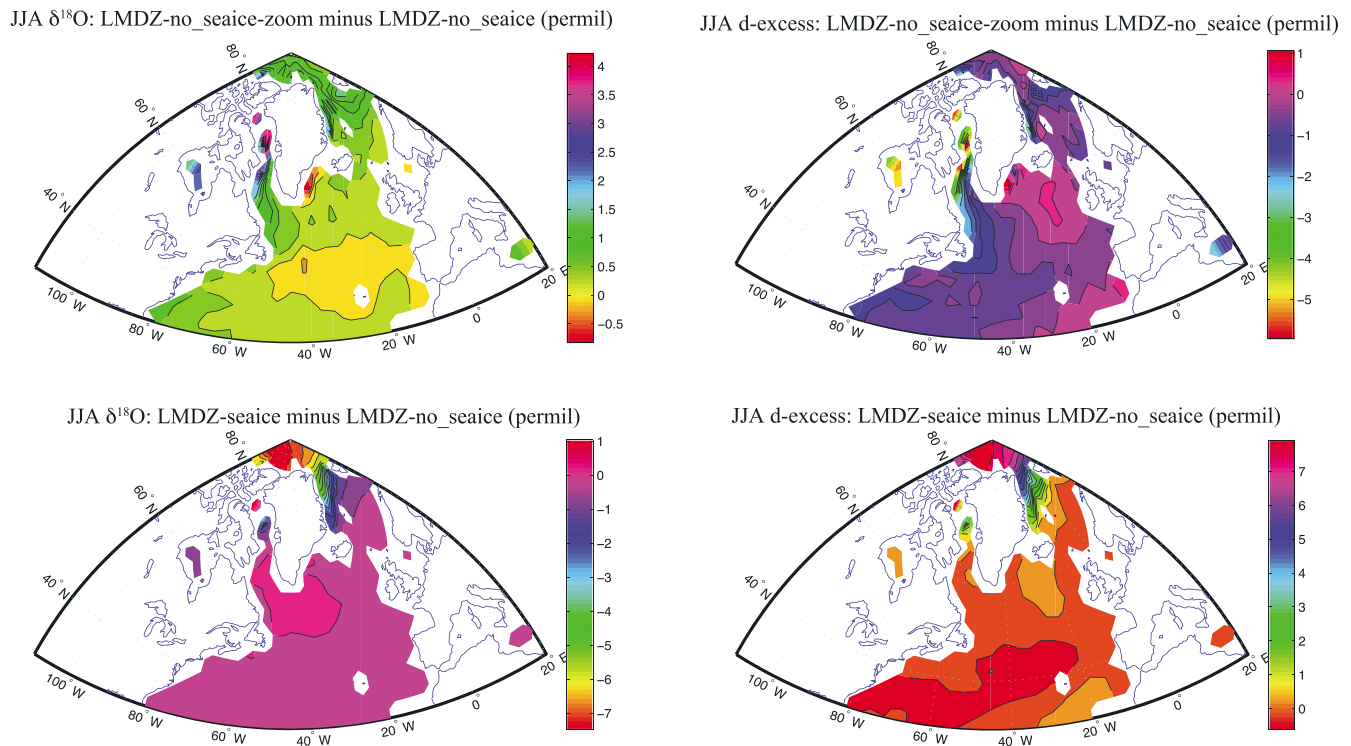


Figure 6. Difference between $\delta^{18}\text{O}$ and d-excess simulated at the first model level by LMDZiso-no_seaice-zoom and LMDZiso-no_seaice.

understand the processes affecting the Baffin Bay surface vapor isotopic composition when model resolution is modified. We do not offer an explanation for the general poleward high latitudinal bias in $\delta^{18}\text{O}$. However, we notice that *Hendricks et al.* [2000] showed that the latitudinal gradient is very sensitive to the proportion of transport by eddies and mixing due to too much diffusivity in the horizontal.

We finally stress the remarkable skill of ECHAM5-wiso in the simulation of the relationship between $\delta^{18}\text{O}$ and humidity for the different marine boundary layer sites and at NEEM (Figure 3). This might be related to the nudging of temperature, pressure, and wind both locally and across the oceanic source regions for the ECHAM5-wiso model, but we are not able to quantify this further here.

4.3. Causes of the Poor Performance for d-Excess

Our comparison shows that all of the five simulations fail to capture the observed mean level and variability of d-excess in surface vapor at NEEM.

First, we attribute the largest simulated variability of isoGSM for NEEM d-excess to the larger spatial variability for d-excess in the surrounding marine boundary layer, ranging from 2‰ southeast of Greenland to 12‰ north of Greenland (compare with 4–8‰, for other models). Moreover, isoGSM produces a strong relationship between d-excess and $\delta^{18}\text{O}$. We therefore speculate that its remarkably low d-excess mean level is related to its lack of $\delta^{18}\text{O}$ depletion at NEEM.

We now focus on LMDZiso simulations, which show better skill for d-excess variability at NEEM than other models. The three simulations with the LMDZiso model show very similar but shifted patterns of d-excess versus $\delta^{18}\text{O}$ (Figure 4). Differences simulated at NEEM are likely related to differences in the marine boundary layer excess, e.g., above the Baffin Bay (Figure 6). The sensitivity of this surface vapor isotopic composition to model resolution may arise from synoptic-scale processes such as polar lows. Given that the relationship between d-excess and $\delta^{18}\text{O}$ becomes steeper for more depleted $\delta^{18}\text{O}$ values, we speculate that a better skill for d-excess variability could be achieved if the simulated $\delta^{18}\text{O}$ level was more realistic. This would therefore require simulating correctly the latitudinal gradient in marine boundary layer $\delta^{18}\text{O}$ (and also d-excess). The LMDZiso-no_seaice/seaice and LMDZiso-no_seaice-zoom simulations stress that an increased resolution of

the atmospheric model is not by itself sufficient: with respect to observations from Bermuda, Iceland, South Greenland, and Svalbard, the model-data mismatch is worse for LMDZiso-no_seaice-zoom than for LMDZiso-no_seaice/seaice (Figures 4 and 6).

We finally attribute the fact that ECHAM5-wiso has the best skill in representing the d-excess versus $\delta^{18}\text{O}$ relationship to the fact that it has the best skill in representing the $\delta^{18}\text{O}$ versus humidity relationships in all marine boundary layer sites. The fact that ECHAM5-wiso fails to capture the NEEM d-excess variability therefore likely arises from problems in the representation of Arctic d-excess.

We expect the simulated d-excess to depend both on the parameterization of the boundary layer and on the number of vertical levels to resolve the planetary boundary layer. Both these factors influence the relative humidity near the surface [Hourdin *et al.*, 2013] and thus the d-excess. The fact that LMDZ has the highest vertical resolution, but does not simulate the d-excess significantly better, suggests that the differences in the simulated d-excess arise mainly from differences in the parameterizations and not from the simulation of the relative humidity at SST (RHsst). At the surface the turbulent flux is obtained from the bulk transfer relationship, which depends on the transfer coefficient, wind speed, and difference between the bulk values of the lowest model level and the surface. The transfer coefficients are determined from Monin-Obukhov similarity theory [e.g., Foken, 2006]. In the planetary boundary layer above the surface layer the eddy fluxes are computed as diffusive fluxes, which are related to the diffusion coefficient and the gradient of the respective variable. The diffusion coefficient depends on height, shear, and stability [e.g., Hourdin *et al.*, 2006; Roeckner *et al.*, 2003; Song-You and Hua-Lu, 1996]. The thermal plume model simulates the organized mixing structures within the boundary layer [Rio and Hourdin, 2008]. It is expected that an increase in vertical eddy fluxes will result in more mixing of the air from the free troposphere into the surface layer. Such an increased mixing will result in a lowering of the isotopic composition of the water vapor in the surface layer but would also result in an increased flux from the ocean surface, which would tend to increase the isotopic composition of the water vapor. Hence, detailed sensitivity studies are needed to address the influence of the model tunable parameters on the marine boundary layer water vapor isotopic composition. This, together with quantifying the role of the planetary boundary layer, is unfortunately outside the scope of this paper.

4.4. Robustness of Model Evaluation With Respect to the Length of the Observations

Here we have performed model-data comparisons for three summer season campaigns (2010–2012). In order to provide guidance for monitoring efforts, we explore the robustness of our findings with respect to the length of the observational record through the comparison of results for each season (Figure 7 and Table S1 in the supporting information). The intermodel dispersion for simulated air temperature, humidity, $\delta^{18}\text{O}$, and d-excess, as well as the model-data biases, can be identified for a single season. Metrics for model-data skills performed based on day-to-day variability may, however, be limited for short measurement seasons (typically less than 60 days).

We conclude that water vapor isotope observations performed during one single summer season can be used to assess model skills and identify outlier behavior. This finding calls for concerted efforts to provide short-lived measurements (campaigns) in areas with large intermodel spread (e.g., Baffin Bay area and Arctic sea ice margin) and to provide simultaneous measurements in other regions, which are critical to track atmospheric transport pathways [e.g., Bonne *et al.*, 2015]. Our data sets are now available for instance to test the added value of model developments or to adjust the tuning of specific parameterizations.

5. Conclusion and Perspectives

Here we have performed the first exercise of model intercomparison using surface vapor isotopic measurements.

We have shown that isotopic biases cannot simply be explained by model artifacts for temperature and humidity but may arise from their inability to correctly simulate the spatial structure of marine boundary layer isotopic composition along a latitudinal North Atlantic-Arctic transect.

We have shown that isoGSM produces a larger spatial variability in surface vapor $\delta^{18}\text{O}$, possibly explaining its large variance simulated at NEEM, and its limited skill at this site. We have also identified a good performance of ECHAM5-wiso for the overall $\delta^{18}\text{O}$ -humidity relationships in the marine boundary layer, and for NEEM $\delta^{18}\text{O}$.

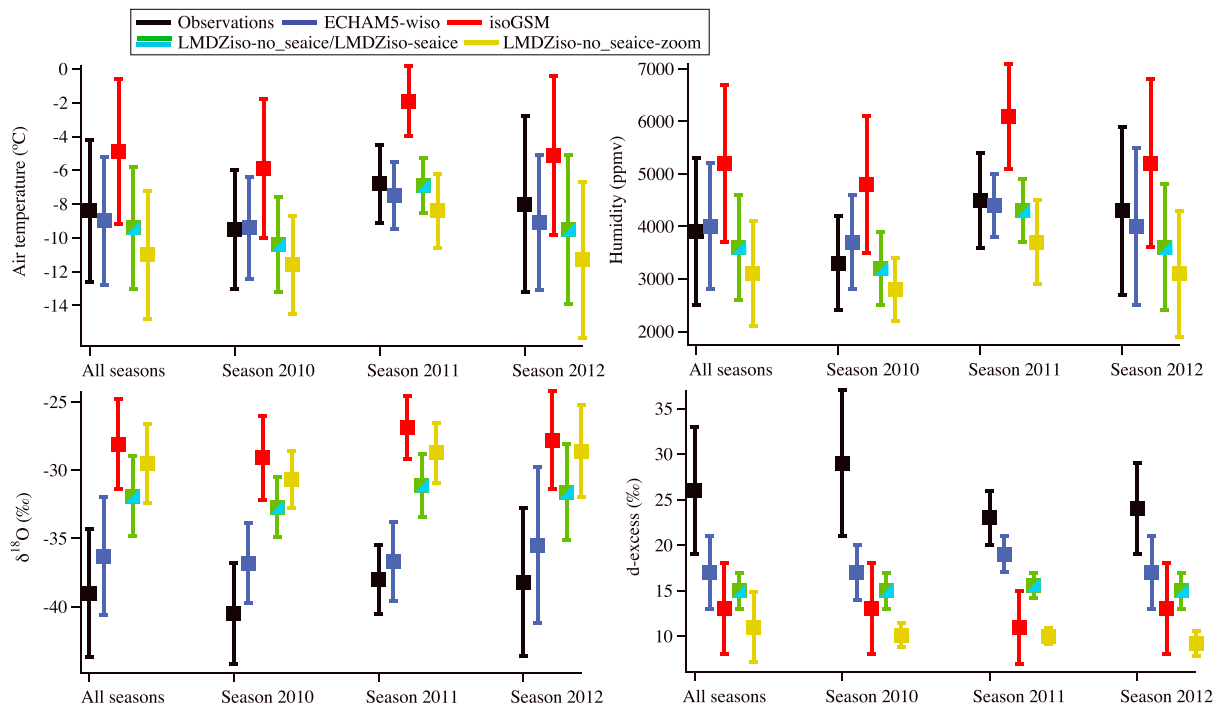


Figure 7. Observed (black) and simulated (colors) characteristics of NEEM surface air temperature, humidity, $\delta^{18}\text{O}$, and d-excess (mean value and standard deviation) calculated for all combined seasons and for individual seasons (2010, 2011, or 2012).

While all models perform poorly for d-excess, LMDZiso appears to resolve some of the day-to-day variations. The comparison of a zoomed and a standard, low resolution simulation suggests that model resolution alone does not improve model performance for water vapor isotopes. It has shown evidence over some areas (e.g., Baffin Bay) where marine boundary layer isotopic composition appears very sensitive to model resolution.

We have also demonstrated that measurements performed at the NEEM site over just one season can provide a basis for model evaluation, thanks to the robustness of model-data results over three summers. We have also stressed the importance of a coordinated monitoring network in order to benchmark the spatial structure of marine boundary layer vapor isotopic composition around Greenland. Given the wide intermodel spread in some areas (e.g., Baffin Bay, Arctic, and east of Newfoundland), further measurement campaigns are highly needed to discriminate amongst these model behaviors.

We have confirmed the inability of state-of-the-art atmospheric isotope-enabled models to capture the mean level as well as the day-to-day variability in surface vapor deuterium excess, both at NEEM and for large-scale North Atlantic/Arctic gradients. This may arise from inadequacies related to, for instance, surface humidity, large-scale moisture transport pathways, or calculations of the isotopic composition at sea ice margins. Our results suggest that models are able to resolve low d-excess values associated with extratropical storms (e.g., the summer 2012 atmospheric river event) but fail to capture the high d-excess of Arctic air masses. Refinements of the modeling of the ocean-sea ice-atmosphere interface for isotopic fluxes may be required. We speculate that issues could arise with the simulation of the moisture content in the near surface layer or in the parameterization of the kinetic fractionation, for example, the influence of wind speed.

We have shown evidence of a number of model shortcomings, both for mean levels and for day-to-day variations within a summer. Further investigations of intermodel spread from the synoptic scale to the seasonal, interannual, decadal, or longer time scales is important to make better use of such present-day model-data comparisons to guide the use of models for the interpretation of paleoclimate records. Our results call for a very cautious use of simulated d-excess, for instance.

Our analyses of relationships between marine boundary layer isotopic composition, transport, and mixing have been preliminary. We suggest that several biases of models at the NEEM location in fact result from

model biases for marine boundary layer isotopic composition. Further investigations will require combining our analysis with diagnostics of moisture origin, using either backward trajectories or moisture tagging tools. We also stress the importance of testing the influence of too high horizontal diffusion in the models and the influence of this process on the latitudinal gradient in the isotopic composition. We speculate that the vertical resolution of the layers near the ocean could influence the humidity level of the simulated air in contact with the ocean and thereby control the isotopic flux through kinetic fractionation.

Finally, this intercomparison stresses the potential use of surface vapor water stable isotopes for the evaluation of the atmospheric water cycle in atmospheric models, including the possibility to test in a coherent framework the performance of different atmospheric analysis products (not done here) and the possibility to test the benefits of increased spatial resolution (explored using LMDZiso-no_seaice-zoom) and to test different model parameterizations (not done).

Acknowledgments

The data used in this manuscript are available in attached Excel sheet. It is recommended to contact H.C. Steen-Larsen (hanschr@gfy.ku.dk) for information about potential limitations in respect to answering a given research question. For model simulations and up-to-date observations from the marine boundary layer vapor isotope stations please contact H.C. Steen-Larsen. The work was supported by the Danish Council for Independent Research–Natural Sciences grants 09–072689 and 10–092850, the Carlsberg Foundation, the AXA Research Fund, and the Agence Nationale de la Recherche ANR AC-AHC2 project (ANR-15-CE01-0015). LMDZ simulations were performed using the HPC resources of IDRIS under the allocation 0292 made by GENCI. NEEEM is directed and organized by the Center of Ice and Climate at the Niels Bohr Institute and U.S. NSF, Office of Polar Programs. It is supported by funding agencies and institutions in Belgium (FNRS-CFB and FWO), Canada (GSC), China (CAS), Denmark (FIST), France (IPEV and INSU/CNRS), Germany (AWI), Iceland (Rannls), Japan (NIPR), Korea (KOPRI), the Netherlands (NWO/ALW), Sweden (VR), Switzerland (SNF), United Kingdom (NERC), and the USA (U.S. NSF, Office of Polar Programs). We thank the Editor and four anonymous reviewers for their constructive criticism, which improved the paper significantly.

References

- Baer, D. S., J. B. Paul, M. Gupta, and A. O'Keefe (2002), Sensitive absorption measurements in the near-infrared region using off-axis integrated-cavity-output spectroscopy, *Appl. Phys. B*, *75*, 261–265, doi:10.1007/s00340-002-0971-z.
- Bailey, A., D. Noone, M. Berkelhammer, H. C. Steen-Larsen, and P. Sato (2015), The stability and calibration of water vapor isotope ratio measurements during long-term deployments, *Atmos. Meas. Tech. Discuss.*, *8*, 5425–5466, doi:10.5194/amtd-8-5425-2015.
- Barkan, E., and B. Luz (2007), Diffusivity fractionations of (H₂O)-O-16/(H₂O)-O-17 and (H₂O)-O-16/(H₂O)-O-18 in air and their implications for isotope hydrology, *Rapid Commun. Mass Spectrom.*, *21*, 2999–3005, doi:10.1002/rcm.3180.
- Benetti, M., G. Reverdin, C. Pierre, L. Merlivat, C. Risi, H. C. Steen-Larsen, and F. Vimeux (2014), Deuterium excess in marine water vapor: Dependency on relative humidity and surface wind speed during evaporation, *J. Geophys. Res. Atmos.*, *119*, 584–593, doi:10.1002/2013JD020535.
- Bolot, M., B. Legras, and E. J. Moyer (2013), Modelling and interpreting the isotopic composition of water vapour in convective updrafts, *Atmos. Chem. Phys.*, *13*, 7903–7935, doi:10.5194/acp-13-7903-2013.
- Bonne, J. L., V. Masson-Delmotte, O. Cattani, M. Delmotte, C. Risi, H. Sodemann, and H. C. Steen-Larsen (2014), The isotopic composition of water vapour and precipitation in Ivittuut, southern Greenland, *Atmos. Chem. Phys.*, *14*, 4419–4439, doi:10.5194/acp-14-4419-2014.
- Bonne, J.-L., et al. (2015), The summer 2012 Greenland heat wave: In situ and remote sensing observations of water vapor isotopic composition during an atmospheric river event, *J. Geophys. Res. Atmos.*, *120*, 2970–2989, doi:10.1002/2014JD022602.
- Compo, G. P., et al. (2011), The twentieth century reanalysis project, *Q. J. R. Meteorol. Soc.*, *137*, 1–28, doi:10.1002/qj.776.
- Craig, H. (1961), Isotopic variations in meteoric waters, *Science*, *133*, 1702–1703.
- Craig, H., and L. I. Gordon (1965), Deuterium and oxygen 18 variations in the ocean and the marine atmosphere, in *Stable Isotopes in Oceanographic Studies and Paleotemperatures*, edited by E. Tongiogi, pp. 9–130, V. Lishi e F., Pisa, Spoleto, Italy.
- Crosson, E. R., et al. (2002), Stable isotope ratios using cavity ring-down spectroscopy: Determination of C-13/C-12 for carbon dioxide in human breath, *Anal. Chem.*, *74*, 2003–2007, doi:10.1021/ac025511d.
- Cruz, F. W., S. J. Burns, I. Karmann, W. D. Sharp, M. Vuille, A. O. Cardoso, J. A. Ferrari, P. L. S. Dias, and O. Viana (2005), Insolation-driven changes in atmospheric circulation over the past 116,000 years in subtropical Brazil, *Nature*, *434*, 63–66.
- Dansgaard, W. (1953), The abundance of ¹⁸O in atmospheric water and water vapour, *Tellus*, *5*, 461–469.
- Dansgaard, W. (1964), Stable isotopes in precipitation, *Tellus*, *16*, 436–468.
- Dee, D. P., et al. (2011), The ERA-Interim reanalysis: Configuration and performance of the data assimilation system, *Q. J. R. Meteorol. Soc.*, *137*, 553–597, doi:10.1002/qj.828.
- Ellehoj, M. D., H. C. Steen-Larsen, S. J. Johnsen, and M. B. Madsen (2013), Ice-vapor equilibrium fractionation factor of hydrogen and oxygen isotopes: Experimental investigations and implications for stable water isotope studies, *Rapid Commun. Mass Spectrom.*, *27*, 2149–2158, doi:10.1002/rcm.6668.
- European Project for Ice Coring in Antarctica Community Members (2006), One-to-one coupling of glacial climate variability in Greenland and Antarctica, *Nature*, *444*, 195–198.
- Epstein, S., and T. Mayeda (1953), Variation of the 18-O content of waters from natural sources, *Geochim. Cosmochim. Acta*, *4*, 213–224.
- Foken, T. (2006), 50 years of the Monin–Obukhov similarity theory, *Boundary Layer Meteorol.*, *119*, 431–447, doi:10.1007/s10546-006-9048-6.
- Galewsky, J., H. C. Steen-Larsen, R. D. Field, J. Worden, C. Risi, and M. Schneider (2016), Stable isotopes in atmospheric water vapor and applications to the hydrologic cycle, *Rev. Geophys.*, *54*, doi:10.1002/2015RG000512.
- Hanna, E., et al. (2013), Ice-sheet mass balance and climate change, *Nature*, *498*, 51–59, doi:10.1038/nature12238.
- Hendricks, M. B., D. J. DePaolo, and R. C. Cohen (2000), Space and time variation of $\delta^{18}\text{O}$ and δD in precipitation: Can paleotemperature be estimated from ice cores?, *Global Biogeochem. Cycles*, *14*, 851–861.
- Hourdin, F., et al. (2006), The LMDZ4 general circulation model: Climate performance and sensitivity to parametrized physics with emphasis on tropical convection, *Clim. Dyn.*, *27*, 787–813, doi:10.1007/s00382-006-0158-0.
- Hourdin, F., et al. (2013), LMDZ5B: The atmospheric component of the IPSL climate model with revisited parameterizations for clouds and convection, *Clim. Dyn.*, *40*, 2193–2222, doi:10.1007/s00382-012-1343-y.
- Johnsen, S. J., W. Dansgaard, and J. W. C. White (1989), The origin of Arctic precipitation under present and glacial conditions, *Tellus B*, *41*, 452–468.
- Jouzel, J., and L. Merlivat (1984), Deuterium and oxygen 18 in precipitation: Modeling of the isotopic effects during snow formation, *J. Geophys. Res.*, *89*, 11,749–11,757, doi:10.1029/JD089iD07p11749.
- Jouzel, J., G. Delaygue, A. Landais, V. Masson-Delmotte, C. Risi, and F. Vimeux (2013), Water isotopes as tools to document oceanic sources of precipitation, *Water Resour. Res.*, *49*, 7469–7486, doi:10.1002/2013WR013508.
- Kanamitsu, M., W. Ebisuzaki, J. Woollen, S. K. Yang, J. J. Hnilo, M. Fiorino, and G. L. Potter (2002), NCEP-DOE AMIP-II reanalysis (R-2), *Bull. Am. Meteorol. Soc.*, *83*, 1631–1643, doi:10.1175/bams-83-11-1631.
- Kurita, N. (2011), Origin of Arctic water vapor during the ice-growth season, *Geophys. Res. Lett.*, *38*, L02709, doi:10.1029/2010GL046064.
- Lee, J. E., I. Fung, D. J. DePaolo, and C. C. Henning (2007), Analysis of the global distribution of water isotopes using the NCAR atmospheric general circulation model, *J. Geophys. Res.*, *112*, D16306, doi:10.1029/2006JD007657.

- Lee, J.-E., I. Fung, D. J. DePaolo, and B. Otto-Bliesner (2008), Water isotopes during the Last Glacial Maximum: New general circulation model calculations, *J. Geophys. Res.*, *113*, D19109, doi:10.1029/2008JD009859.
- LeGrande, A. N., and G. A. Schmidt (2006), Global gridded data set of the oxygen isotopic composition in seawater, *Geophys. Res. Lett.*, *33*, L12604, doi:10.1029/2006GL026011.
- LeGrande, A. N., and G. A. Schmidt (2009), Sources of Holocene variability of oxygen isotopes in paleoclimate archives, *Clim. Past*, *5*, 441–455, doi:10.5194/cp-5-441-2009.
- Majoube, M. (1970), Fractionation factor of ^{18}O between water vapour and ice, *Nature*, *226*, 1242.
- Majoube, M. (1971), Fractionnement en oxygène 18 et en deutérium entre l'eau et sa vapeur, *J. Clim. Phys.*, *68*, 1423–1436.
- Masson-Delmotte, V., et al. (2005), Holocene climatic changes in Greenland: Different deuterium excess signals at Greenland Ice Core Project (GRIP) and NorthGRIP, *J. Geophys. Res.*, *110*, D14102, doi:10.11029/12004JD005575.
- Masson-Delmotte, V., et al. (2011), Sensitivity of interglacial Greenland temperature and delta(^{18}O): Ice core data, orbital and increased CO(2) climate simulations, *Clim. Past*, *7*, 1041–1059, doi:10.5194/cp-7-1041-2011.
- Masson-Delmotte, V., et al. (2015a), Recent changes in north-west Greenland climate documented by NEEM shallow ice core data and simulations, and implications for past-temperature reconstructions, *Cryosphere*, *9*, 1481–1504, doi:10.5194/tc-9-1481-2015.
- Masson-Delmotte, V., H. C. Steen-Larsen, N. Zanetti, O. Cattani, M. Maturilli, S. Debatin, S. Terzer, J. L. Bonne, and M. Schneider (2015b), Understanding climatic controls on Svalbard water vapour and precipitation isotopic composition, EGU, EGU2015-14482-14481.
- Merlivat, L., and J. Jouzel (1979), Global climatic interpretation of the deuterium-oxygen 18 relationship for precipitation, *J. Geophys. Res.*, *84*, 5029–5033, doi:10.1029/JC084iC08p05029.
- Merlivat, L., and G. Nief (1967), Fractionnement isotopique lors des changements d'état solide-vapeur et liquide-vapeur de l'eau à des températures inférieures à 0°C, *Tellus*, *1*, 122–127.
- Merz, N., C. C. Raible, H. Fischer, V. Varma, M. Prange, and T. F. Stocker (2013), Greenland accumulation and its connection to the large-scale atmospheric circulation in ERA-Interim and paleoclimate simulations, *Clim. Past*, *9*, 2433–2450, doi:10.5194/cp-9-2433-2013.
- NEEM Community Members (2013), Eemian interglacial reconstructed from a Greenland folded ice core, *Nature*, *493*, 489–494, doi:10.1038/nature11789.
- North Greenland Ice-Core Project Members (2004), High resolution climate record of the Northern Hemisphere reaching into the last Glacial Interglacial Period, *Nature*, *431*, 147–151.
- Okazaki, A., Y. Satoh, G. Tremoy, F. Vimeux, R. Scheepmaker, and K. Yoshimura (2015), Interannual variability of isotopic composition in water vapor over western Africa and its relationship to ENSO, *Atmos. Chem. Phys.*, *15*, 3193–3204, doi:10.5194/acp-15-3193-2015.
- Ortega, P., F. Lehner, D. Swingedouw, V. Masson-Delmotte, C. C. Raible, M. Casado, and P. Yiou (2015), A model-tested North Atlantic Oscillation reconstruction for the past millennium, *Nature*, *523*, 71–74, doi:10.1038/nature14518.
- Pfahl, S., H. Wernli, and K. Yoshimura (2012), The isotopic composition of precipitation from a winter storm—A case study with the limited-area model COSMOiso, *Atmos. Chem. Phys.*, *12*, 1629–1648, doi:10.5194/acp-12-1629-2012.
- Rio, C., and F. Hourdin (2008), A thermal plume model for the convective boundary layer: Representation of cumulus clouds, *J. Atmos. Sci.*, *65*, 407–425, doi:10.1175/2007jas2256.1.
- Risi, C., S. Bony, F. Vimeux, and J. Jouzel (2010), Water stable isotopes in the LMDZ4 general circulation model: Model evaluation for present day and past climates and applications to climatic interpretations of tropical isotopic records, *J. Geophys. Res.*, *115*, D12118, doi:10.1029/2009JD013255.
- Risi, C., et al. (2012), Process-evaluation of tropospheric humidity simulated by general circulation models using water vapor isotopologues: 1. Comparison between models and observations, *J. Geophys. Res.*, *117*, D05303, doi:10.1029/2011JD016621.
- Ritter, F., H. C. Steen-Larsen, M. Werner, V. Masson-Delmotte, A. Orsi, M. Behrens, G. Birnbaum, J. Freitag, C. Risi, and S. Kipfstuhl (2016), Isotopic exchange on the diurnal scale between near-surface snow and lower atmospheric water vapor at Kohonen station, East Antarctica, *The Cryosphere*, *10*, 1647–1663, doi:10.5194/tc-10-1647-2016.
- Roeckner, E., et al. (2003), The atmospheric general circulation model ECHAM5. Part I: Model description., Available from MPI for Meteorology, Bundesstr. 53, 20146 Hamburg, Germany., 127.
- Schoenemann, S. W., E. J. Steig, Q. Ding, B. R. Markle, and A. J. Schauer (2014), Triple water-isotopologue record from WAIS Divide, Antarctica: Controls on glacial-interglacial changes in ^{17}O excess of precipitation, *J. Geophys. Res. Atmos.*, *119*, 8741–8763, doi:10.1002/2014JD021770.
- Schoenemann, K. C., and J. J. Cassano (2009), Changes in synoptic weather patterns and Greenland precipitation in the 20th and 21st centuries: 1. Evaluation of late 20th century simulations from IPCC models, *J. Geophys. Res.*, *114*, D20113, doi:10.1029/2009JD011705.
- Sime, L. C., C. Risi, J. C. Tindall, J. Sjolte, E. W. Wolff, V. Masson-Delmotte, and E. Capron (2013), Warm climate isotopic simulations: What do we learn about interglacial signals in Greenland ice cores?, *Quat. Sci. Rev.*, *67*, 59–80, doi:10.1016/j.quascirev.2013.01.009.
- Sjolte, J., G. Hoffmann, S. J. Johnsen, B. M. Vinther, V. Masson-Delmotte, and C. Sturm (2011), Modeling the water isotopes in Greenland precipitation 1959–2001 with the meso-scale model REMO-iso, *J. Geophys. Res.*, *116*, D18105, doi:10.1029/2010JD015287.
- Song-You, H., and P. Hua-Lu (1996), Nonlocal boundary layer vertical diffusion in a medium-range forecast model, *Mon. Weather Rev.*, *124*, 2322–2339, doi:10.1175/1520-0493(1996)124<2322:NBLVDI>2.0.CO;2.
- Steen-Larsen, H. C., et al. (2011), Understanding the climatic signal in the water stable isotope records from the NEEM shallow firn/ice cores in northwestern Greenland, *J. Geophys. Res.*, *116*, D06108, doi:10.1029/2010JD014311.
- Steen-Larsen, H. C., et al. (2013), Continuous monitoring of summer surface water vapor isotopic composition above the Greenland Ice Sheet, *Atmos. Chem. Phys.*, *13*, 4815–4828, doi:10.5194/acp-13-4815-2013.
- Steen-Larsen, H. C., et al. (2014a), What controls the isotopic composition of Greenland surface snow?, *Clim. Past*, *10*, 377–392, doi:10.5194/cp-10-377-2014.
- Steen-Larsen, H. C., A. E. Sveinbjörnsdóttir, A. J. Peters, V. Masson-Delmotte, M. P. Guishard, G. Hsiao, J. Jouzel, D. Noone, J. K. Warren, and J. W. C. White (2014b), Climatic controls on water vapor deuterium excess in the marine boundary layer of the North Atlantic based on 500 days of in situ, continuous measurements, *Atmos. Chem. Phys.*, *14*, 7741–7756, doi:10.5194/acp-14-7741-2014.
- Steen-Larsen, H. C., A. E. Sveinbjörnsdóttir, T. Jonsson, F. Ritter, J. L. Bonne, V. Masson-Delmotte, H. Sodemann, T. Blunier, D. Dahl-Jensen, and B. M. Vinther (2015), Moisture sources and synoptic to seasonal variability of North Atlantic water vapor isotopic composition, *J. Geophys. Res. Atmos.*, *120*, 5757–5774, doi:10.1002/2015JD023234.
- Steffensen, J. P., et al. (2008), High-resolution Greenland Ice Core data show abrupt climate change happens in few years, *Science*, *321*, 680–684, doi:10.1126/science.1157707.
- Stewart, M. K. (1975), Stable isotope fractionation due to evaporation and isotopic exchange of falling waterdrops: Applications to atmospheric processes and evaporation of lakes, *J. Geophys. Res.*, *80*, 1133–1146, doi:10.1029/JC080i009p01133.

- Sturm, K., G. Hoffmann, B. Langmann, and W. Stihler (2005), Simulation of delta O-18 in precipitation by the regional circulation model REMOiso, *Hydrol. Processes*, *19*, 3425–3444, doi:10.1002/hyp.5979.
- Taylor, K. E. (2001), Summarizing multiple aspects of model performance in a single diagram, *J. Geophys. Res.*, *106*, 7183–7192, doi:10.1029/2000JD900719.
- Tindall, J. C., P. J. Valdes, and L. C. Sime (2009), Stable water isotopes in HadCM3: Isotopic signature of El Niño Southern Oscillation and the tropical amount effect, *J. Geophys. Res.*, *114*, D04111, doi:10.1029/2008JD010825.
- Treydte, K., et al. (2007) Signal strength and climate calibration of a European tree-ring isotope network, *Geophys. Res. Lett.*, *34*, L24302, doi:10.1029/2007GL031106.
- Uemura, R., V. Masson-Delmotte, J. Jouzel, A. Landais, H. Motoyama, and B. Stenni (2012), Ranges of moisture-source temperature estimated from Antarctic ice cores stable isotope records over glacial–interglacial cycles, *Clim. Past*, *8*, 1109–1125, doi:10.5194/cp-8-1109-2012.
- Vernon, C. L., J. L. Bamber, J. E. Box, M. R. van den Broeke, X. Fettweis, E. Hanna, and P. Huybrechts (2013), Surface mass balance model intercomparison for the Greenland ice sheet, *Cryosphere*, *7*, 599–614, doi:10.5194/tc-7-599-2013.
- Walsh, J. E., W. L. Chapman, V. Romanovsky, J. H. Christensen, and M. Stendel (2008), Global climate model performance over Alaska and Greenland, *J. Clim.*, *21*, 6156–6174, doi:10.1175/2008JCLI2163.1.
- Wang, X.-F., and D. Yakir (2000), Using stable isotopes of water in evapotranspiration studies, *Hydrol. Processes*, *14*, 1407–1421, doi:10.1002/1099-1085(20000615)14:8<1407::AID-HYP992>3.0.CO;2-K.
- Wang, Y., H. Cheng, R. L. Edwards, X. Kong, X. Shao, S. Chen, J. Wu, X. Jiang, X. Wang, and Z. An (2008), Millennial- and orbital-scale changes in the East Asian monsoon over the past 224,000 years, *Nature*, *451*, 1090–1093, doi:10.1038/nature06692.
- Wei, Z., K. Yoshimura, A. Okazaki, K. Ono, W. Kim, M. Yokoi, and C.-T. Lai (2016), Understanding the variability of water isotopologues in near-surface atmospheric moisture over a humid subtropical rice paddy in Tsukuba, Japan, *J. Hydrol.*, *533*, 91–102, doi:10.1016/j.jhydrol.2015.11.044.
- Werner, M., M. Heimann, and G. Hoffmann (2001), Isotopic composition and origin of polar precipitation in present and glacial climate simulations, *Tellus B*, *53*, 53–71.
- Werner, M., P. M. Langebroek, T. Carlsen, M. Herold, and G. Lohmann (2011), Stable water isotopes in the ECHAM5 general circulation model: Toward high-resolution isotope modeling on a global scale, *J. Geophys. Res.*, *116*, D15109, doi:10.1029/2011JD015681.
- Yoshimura, K. (2015), Stable water isotopes in climatology, meteorology, and hydrology: A review, *J. Meteorol. Soc. Jpn. Ser. II*, *93*, 513–533, doi:10.2151/jmsj.2015-036.
- Yoshimura, K., and M. Kanamitsu (2008), Dynamical global downscaling of global reanalysis, *Mon. Weather Rev.*, *136*, 2983–2998, doi:10.1175/2008MWR2281.1.
- Yoshimura, K., M. Kanamitsu, D. Noone, and T. Oki (2008), Historical isotope simulation using reanalysis atmospheric data, *J. Geophys. Res.*, *113*, D19108, doi:10.1029/2008JD010074.
- Yoshimura, K., M. Kanamitsu, and M. Dettinger (2010), Regional downscaling for stable water isotopes: A case study of an atmospheric river event, *J. Geophys. Res.*, *115*, D18114, doi:10.1029/2010JD014032.